# 18th Australian International Aerospace Congress

***Please select category below:***
Normal Paper ☒
Student Paper ☐
Young Engineer Paper ☐


# Accurate Osculating/Mean Orbital Elements Conversions for Spaceborne Formation Flying


Gabriella Gaias [1], Martin Lara [2], and Camilla Colombo [1]

[1] *Department of Aerospace Science and Technology, Politecnico di Milano, 20156 Milano, Italy*
[2] *GRUCACI, University of La Rioja, 26006 Logroño, Spain*



## Abstract

This work addresses the two-way conversion between osculating and mean orbital elements, as required by orbital elements-based onboard guidance navigation and control algorithms for near-circular formation flying missions in low Earth orbits. With regard to the non-homogenous Earth mass distribution perturbation, the developed algorithm merges a Hamiltonian approach applied to the $J_2$ problem with Kaula's linear perturbation method for the remaining terms of the geopotential. Adopting such transformations, the relative motion – analytically propagated in the domain of the linearized mean problem – remains accurate over several orbits periods of time, regardless the time when the initialisation occurred. The paper presents the modelling accuracy that can be achieved under realistic operational conditions.



**Keywords:** Formation Flying, Mean Orbital Elements, Analytical Orbital Theories, Relative Motion, Autonomy.


## Introduction

In formation flying applications, orbital elements-based parametrisations of the relative dynamics are often employed to develop Guidance Navigation and Control (GNC) algorithms since they offer several practical advantages, among which the reduction of linearisation errors when expanding the motion with respect to the orbit of the *chief* satellite, and the exploitation of celestial mechanics methods to introduce the effects of orbit correction manoeuvres. In this framework, working in the domain of *mean* Orbital Elements (OEs), intended as the elements' set where short- and long-term periodic oscillations generated by a given orbital perturbation are removed, is very convenient since the relative dynamics has only to reflect the remaining relative secular variations. In the case that the perturbation is solely the one produced by the first not null zonal term of the Earth geopotential (i.e., the $J_2$), for example, the first order expansion of the time derivatives of mean OEs generates a linearised dynamics for which a closed-form state transition matrix can be written, as shown in Refs. 1 and 2, depending on which OE-based state variable is used and on additional assumptions on the eccentricity of the chief's orbit. Subsequently, for guidance and control purposes, the Gauss's variational equations can be used for the mean dynamics, exploiting the fact that the Jacobian expressing the transformation between osculating and mean orbit elements can be reasonably approximated by the identity matrix, as the off-diagonal terms are of order of $J_2$ or smaller [3]. As a result, efficient GNC algorithms can be designed as the ones used by the NASA's MMS (Magnetospheric Multiscale) mission [4] or the ones by DLR's

AVANTI (Autonomous Vision Approach Navigation and Target Identification) in-orbit demonstration of autonomous noncooperative rendezvous [5].

In the low Earth orbit (LEO) region, the absolute motion of a satellite is generally estimated by onboard filtering the GPS-based position data, using numerical integration of the equations of motion, to provide the absolute Cartesian state in an Earth-centred inertial reference frame [6]. In principle, one could directly estimate the mean elements [7], but the first way is a very established approach, often already available in a satellite embarking a GPS receiver with no need to develop any ad-hoc additional flight software. Thus, if one considers that an estimation of the absolute orbit of the chief satellite is accessible and an OE-based formulation is used for the relative GNC algorithms, a proper interfacing is then needed to bridge such functionalities. Interfaces include the handling of rotations to/from the involved reference systems, the computation of osculating OEs, and the two-way osculating/mean OEs conversions.

The computation of mean OEs is based on averaging techniques and nowadays it is required for simultaneous precise long-term orbit propagation of several satellites exploiting semi-numerical and semi-analytical techniques. The survey in Ref. 8 presents an overview of available analytical orbital theories depending on included perturbations and orbit typologies. Compared to this customary use, the computation of mean OEs for formation flying applications, can accept a less accurate result. On the one hand, in fact, the satellites lie in neighbouring orbits and, therefore, part of the conversion-error cancels as soon as one regards the *relative* mean OEs. On the other hand, the typical propagation time-scales between orbit corrections rarely exceed few days, especially when the satellites are very close to each other. On the contrary, the most critical requirement for close formation flying applications is related to the high level of autonomy of the onboard relative GNC system. Accordingly, simple and computationally light algorithms are preferred also for carrying out the OE conversions.

As this work focuses on the LEO region, only the orbital perturbations due to the non-homogenous Earth mass distribution is considered. Moreover, the orbits are characterized by small values of eccentricity, making it reasonable to exploit the near-circular orbit assumption. The presented algorithm adopts the non-singular set of OEs (i.e., zero-inclinations orbits are hardly used in LEO), with the mean argument of latitude for the satellite anomaly component. This set, in fact, allows a straightforward interfacing to the relative GNC algorithms developed in the Relative Orbital Elements (ROEs) as defined in Ref. 2 and used within AVANTI [5].

The paper is structured as follows. First, the interfacing function of the osculating/mean OE conversions is recalled, emphasizing their impact on the *realistic* assessment of the accuracy of the relative motion modelling. Second, a comparison of the conversion accuracy through different satellite theories is performed, when only the $J_2$ term is considered. Based on this trade-off, the proposed algorithm is explained. It employs a second-order Lie-series based approach, analytically derived up to certain order expansion of the $e\,J_2$ term (being $e$ the chief orbit eccentricity), to cancel the short- and long-periodic terms due to the dominant $J_2$ coefficient. Afterwards, the semi-major axis component only is refined through the first-order Kaula method up to the required order and degree term of the geopotential. Last, the paper provides the achievable relative position and velocity error, measured against a given *reference* dynamics, depending on the geopotential terms accounted in the transformations, for 1-day and 2-day long propagation legs. Once computed the initial mean ROEs, the relative motion uses two possible fist-order closed-form state transition matrices. The errors are measured through an index that accounts for the worst-case error in the initial conditions within one orbit, thus providing a realistic conservative assessment of the accuracy achievable by spaceborne executions.

## Body of the Paper

### Osculating/Mean Orbital Elements Conversions

Fig. 1 presents the functional overview of a GNC system where the chief orbit is given as position and velocity state in an Earth-centred inertial system, whereas the relative algorithms – represented by white-background boxes – are developed in OEs [9]. The double-colour-background boxes identify the bridging blocks that encode time synchronisation, reference systems' conversions, OEs computation from/to inertial state, and osculating/mean OE conversions. This work focuses on the latter task and for any component $\kappa$ of the OE set, the osculating (i.e., *osc*) value is related to the mean one according to:

$$\kappa_{\mathrm{osc}} = \kappa_0 + (\delta\kappa)_{\mathrm{sp}} + (\delta\kappa)_{\mathrm{lp}} + \dot{\kappa}_{\mathrm{sec}} t \tag{1}$$

where the subscripts *sec*, *sp*, and *lp* respectively denote secular, short-periodic and long-periodic contributions, function of the mean elements, generated by a given orbital perturbation. The computation of the osculating set $\mathbf{z} = f(\boldsymbol{x})$, with $\boldsymbol{x}$ indicating the mean OEs, using Eqn 1 is referred as to *direct* transformation (i.e., mean-to-osculating or m2o in Fig. 1). On the contrary, the extraction of the mean elements from the osculating set is referred as to the *inverse* transformation (i.e., osculating-to-mean or o2m in Fig. 1). By following the connections linking the blocks, of the guidance (i.e., view a) or of the navigation (i.e., view b) sets-up, one can visualize the different sources of modelling errors that affect the overall accuracy of the system. Here the focus is on minimizing the error sources $\varepsilon_1$ and $\varepsilon_4$, which generate an artificial error component in the initial conditions of the relative dynamics (i.e., $\varepsilon_1$), as well as a contribution to the $(\tilde{y}_{\mathrm{EME}} - y_{\mathrm{EME}})$ or $(\hat{h} - h)$ errors (i.e., $\varepsilon_1$ and $\varepsilon_4$ cumulative effect).

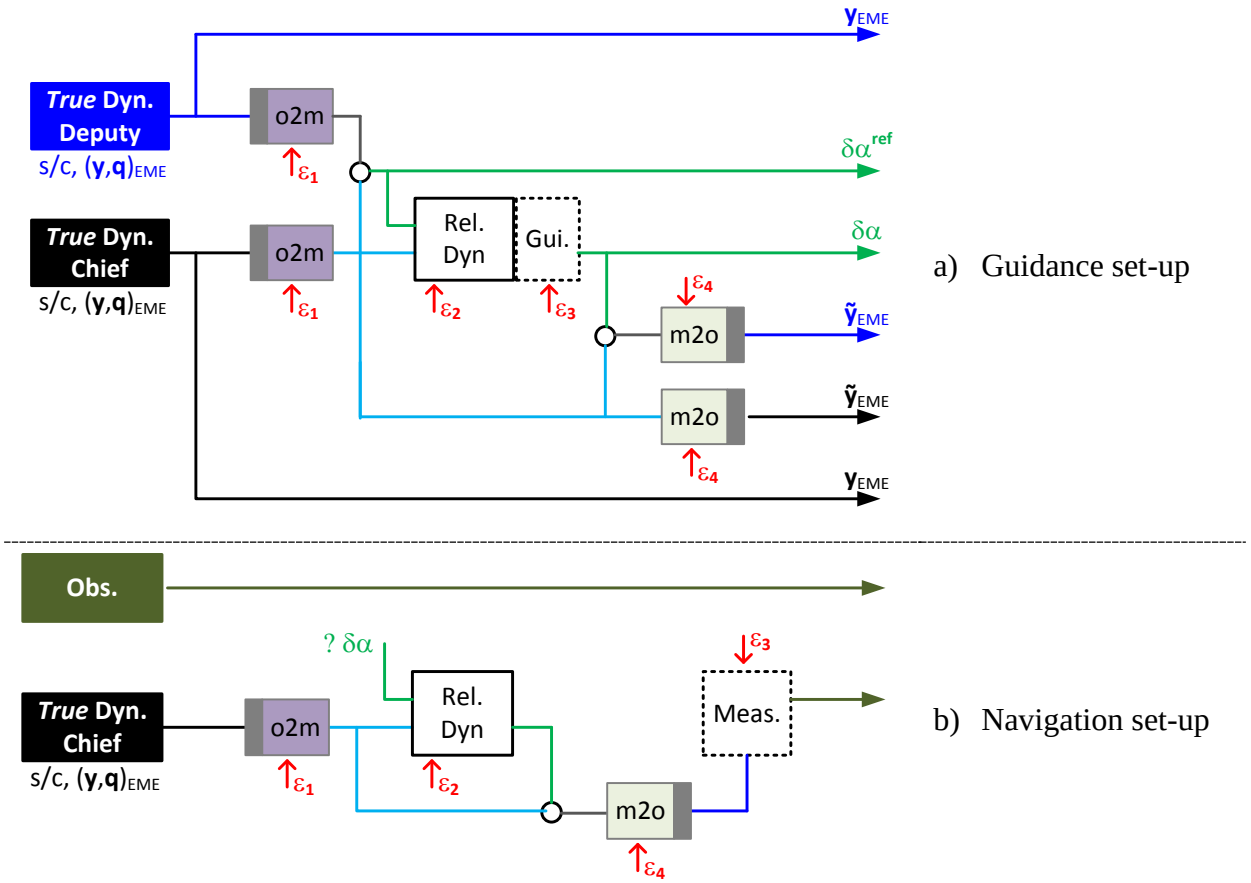


*Fig. 1: Need of osculating/mean conversions to interface the chief absolute orbit to OE-based relative GNC system [9].*

## Comparison of considered approaches

This section presents a set of possible approaches to perform the osculating/mean OE transformations. To the end of comparing their accuracy, the focus is restricted to the $J_2$ problem, thus accounting for only the order-2 degree-0 (i.e., the $-C_{20}$ using Kaula notation [10]) term of the geopotential.

The first approach investigated, labelled as **M-1st**, is the first order mapping described in Appendix F of [3] and used in the flight software of the AVANTI experiment [5]. Such method is based on Brouwer's satellite theory [11] with Lyddane's modification [12] to accommodate small eccentricity and small inclination orbits. Due to the first order truncation, direct and inverse transformations simply differ by a sign.

The remaining considered approaches either require a numerical iterative computation for the inverse transformation or an analytical derivation of some intermediate steps. Both are detailed in the following.

*Iterative method*

The numerical method used in this paper is based on classical fixed-point iterations as originally proposed by Refs. 13 and 14. Accordingly,

$$\begin{aligned} \boldsymbol{x}_{n=0} &= \boldsymbol{z}_{\text{target}} \\ \boldsymbol{x}_{n+1} &= \boldsymbol{x}_n - \boldsymbol{\lambda}\left(f(\boldsymbol{x}_n) - \boldsymbol{z}_{\text{target}}\right) \end{aligned} \tag{2}$$

where the loop is initialized using the known $\mathbf{z}_{\text{target}}$ osculating elements, $\boldsymbol{\lambda}=\mathbf{I}_{1x6}$ [14], and the function *f*, encoding the direct transformation, can derive from different orbital theories. In order to ease the convergence process, the non-singular OEs set with mean argument of latitude as last component is used. Moreover, the semi-major axis component (i.e., *a*) is normalized using the known osculating value. In this way the threshold determining the terminating condition $max(|\boldsymbol{z}_{\text{target}} - \boldsymbol{z}_n|)$ can be set to 1e-8 and generally satisfied within three iterations.

Regarding the comparison the following theories are considered: Brouwer (labelled **B-I**) [11], Kaula linear method (labelled **K-I**) [10], and Eckstein near-circular formulation (labelled **E-I**) [15]. In the labels I stands for *iterative*. More in details,

- In **B-I**, the short- and long-periodic corrections of Eqn 1 are taken from Ref. 11 though using Lyddane's modification. As here the conversion at same time is addressed, the secular motion is not considered. The periodic corrections are due to $J_2$ to the first order. The formulation cannot be used in the vicinity of the critical inclination and the solution of Kepler's equation is needed at every iteration.
- In **K-I**, the short- and long-periodic corrections of Eqn 1 are taken from the linear perturbation method of Ref. 10 generated only by the order-2 degree-0 term and written in the non-singular elements' formulation. Although the direct and inverse transformations differ simply by a sign, the direct function *f* is embedded in the iterative set-up. As it will be shown in the sequel, this allows enforcing – up to the fixed threshold – the maximum cumulative two-way transformation error in the inertial state.
- In **E-I**, the short- and long-periodic corrections of Eqn 1 are taken from Ref. 15 which presents a second order satellite theory suitable for near-circular orbits (eccentricity of the order of the $J_2$), improving the one originally developed by Ustinov in [16]. Although Ref. 15 is developed to consider zonal terms up to order-6 and tesseral terms up to oder-4 degree-4, here only the corrections related to the $J_2$ are considered. In particular, short-periodic corrections include terms of $J_2$, $J_2 e$, and $J_2^2$ (this latter only for the semi-major axis); whereas the long-periodic ones include terms of $J_2$ and $J_2$.

*Analytical method*

The analytical solution of the $J_2$ problem is computed using Hamiltonian perturbation theory by Lie transforms [17]. In particular, three consecutive canonical transformations are applied to obtain the secular terms of the solution up to the third order of $J_2$, whereas the periodic terms are computed up to the second order of $J_2$.

Thus, the elimination of the parallax [18, 19, 20] is applied first to remove non-essential short-period effects from the original Hamiltonian. This pre-processing casts the Hamiltonian into a suitable form that eases the complete removal of the mean anomaly up to higher orders in a following Delaunay normalization [21]. A final Lie transformation eliminates the remaining long-period terms, which are related to the argument of the perigee, yielding a completely reduced, integrable Hamiltonian from which the secular frequencies are easily derived.

The analytical solution constructed in this way is free from singularities related to equatorial or circular orbits, yet it cannot cope with the critical inclination resonance. All the transformations have been computed in closed form of the eccentricity. However, in view of the solution is only applied to the case of low Earth orbits, for better efficiency in the evaluation the periodic corrections have been expanded in powers of the eccentricity. Thus, the first order corrections are accurate to the order of $J_2 e^3$, whereas the second order corrections are accurate to the order of $J_2^2 e$.

In the following, the analytical transformations including solely the first order corrections are labelled **A-1st**, whereas the ones up to second order are labelled **A-2nd**. In the labels A stands for *analytical*.

*Comparison results*

In order to compare the performances of the approaches, a reference scenario of a near-circular (i.e., $e$ = 0.001) orbit at 500 km of height is considered. This orbit is propagated through numerical integration (DO-PRI8, fixed step of 10 s) of the equations of motion subject to $J_2$ only. At each step, the inertial state, in the True-Of-Date (TOD) reference system, is transformed into osculating elements, which then represent the *true* set $\boldsymbol{z}_{\text{target}}(t)$. The cumulative error in position and velocity introduced by the sequence of inverse and direct transformations is then computed as:

$$\boldsymbol{e}(t) = \boldsymbol{y}_{\text{TOD}}(t) - g\left(f\left(\boldsymbol{x}(t)\right)\right), \quad \boldsymbol{x}(t) = f^{-1}\left(\boldsymbol{z}_{\text{target}}(t)\right) \tag{3}$$

Here $g$ denotes the computation of the inertial position and velocity state from the osculating OEs, whereas $f^{-1}$ is the inverse transformation through a given method.

Fig. 2 shows the error of Eqn 3 obtained over one orbital period. Of course, when an iterative approach is used, the error is met to the prescribed tolerance. Thus, only the first-order mapping **M-1st** and the analytical methods may introduce an error greater than the considered tolerance threshold to terminate the iterative loop of Eqn 2.

Fig. 3 shows the corresponding mean elements $\boldsymbol{x}$, resulting from the inverse transformation at each step. One can note that their values vary over the one orbit period time, as result of the transformation error and of the matching imposed by the iterative process. The fact that the conversion error depends on when it is carried out is a relevant aspect for those spaceborne GNC algorithms executed at non-recurring time ticks. In addition, the size of the error depends on the accuracy of the transformation method, with the two second-order approaches (i.e., **E-I** and **A-2nd**) achieving better results. For the anomalies, the plot shows the values to the net of the secular effect, which is obtained through linear fitting of the corresponding data.

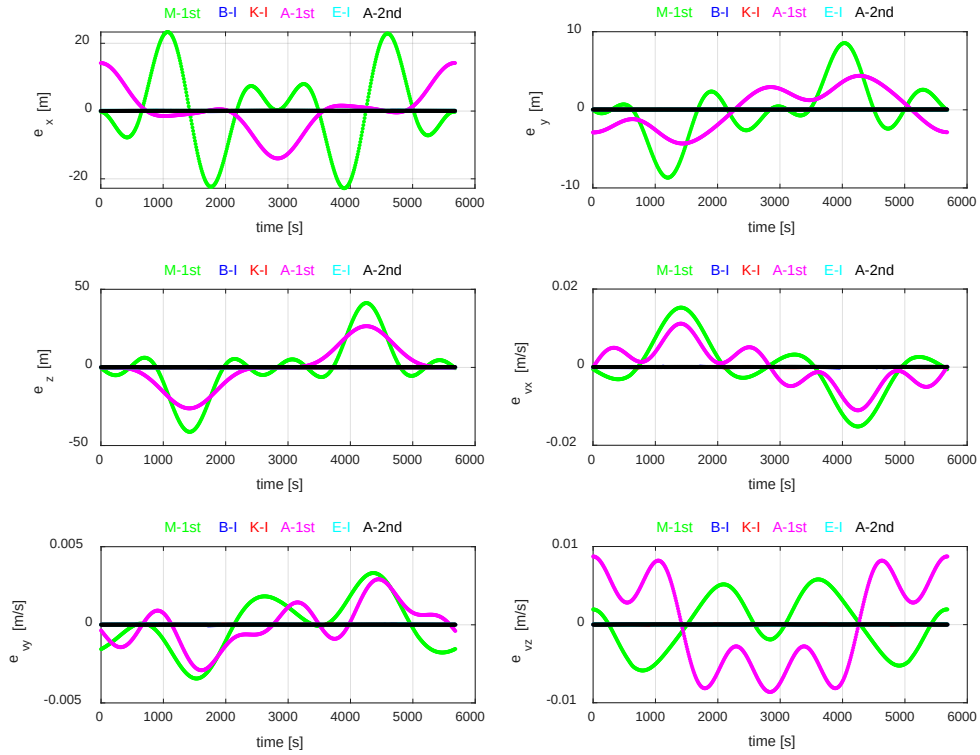


*Fig. 2: Position and velocity error (TOD) from inverse-direct transformation chain.*

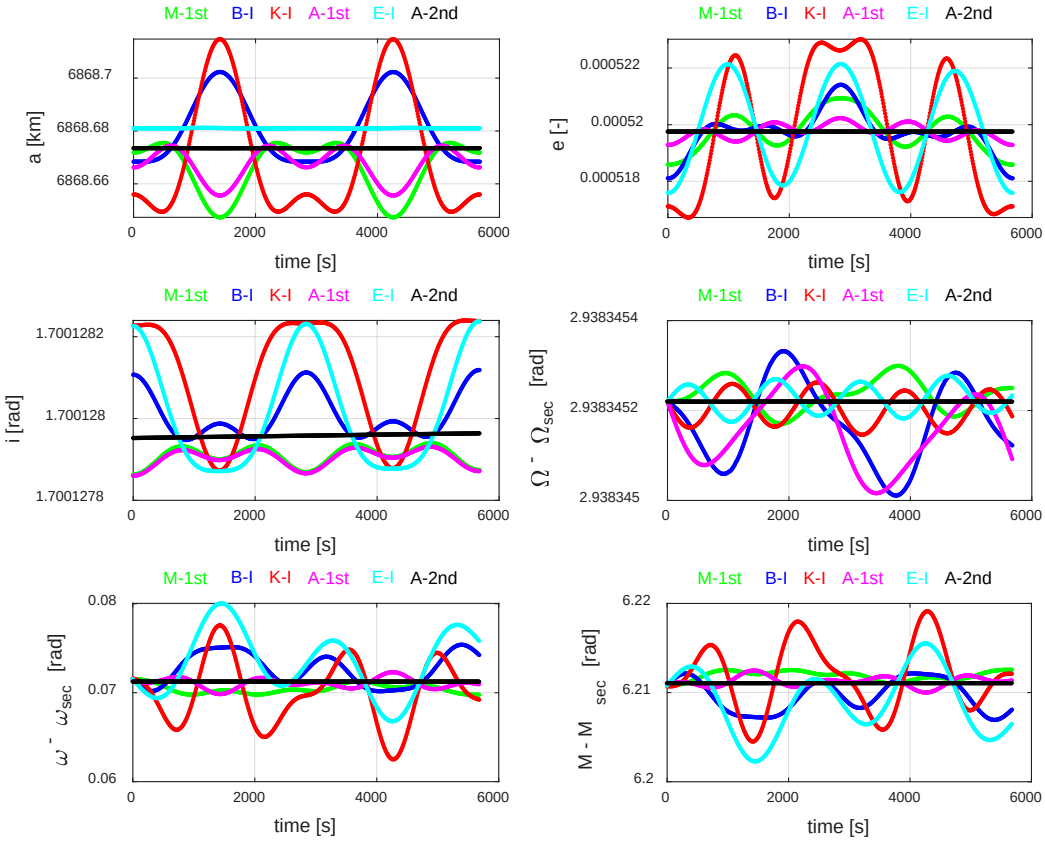


*Fig. 3: Mean elements over time (1 orbit) obtained from inverse transformation.*

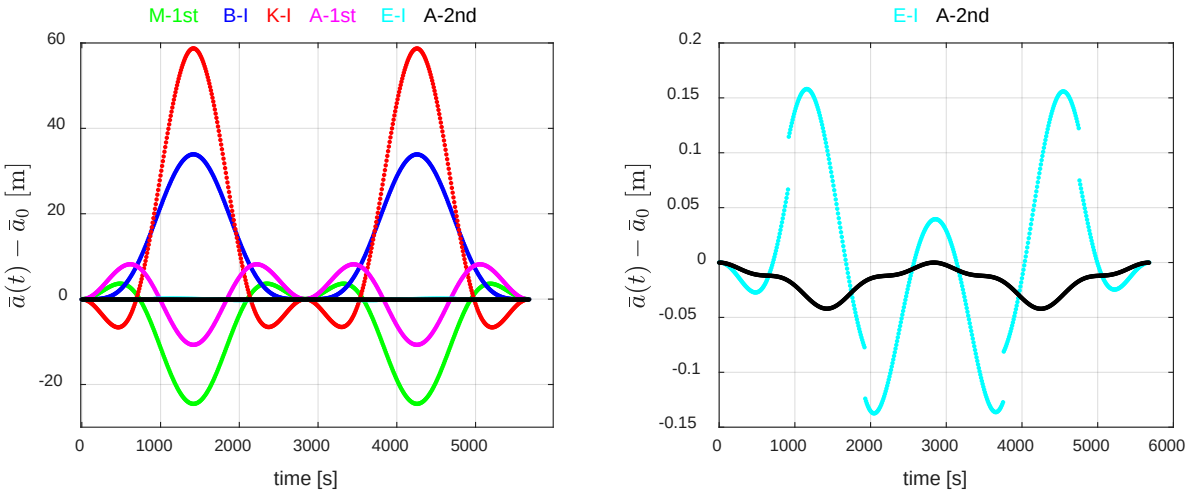


a) All considered methods. b) Only 2nd order methods.

*Fig. 4: Semi-major axis component, plotting its value minus mean value at initial time.*

Dealing with formation-flying, the focus is on the relative motion and thus on the difference of the transformation error between the chief and the deputy orbits. Clearly, part of the absolute conversion error is cancelled by the fact that the orbits are indeed similar. Nevertheless, the bigger the oscillation in mean-value the larger the relative error may be. With reference to Fig. 3, the variation of mean-values for all the components except for the semi-major axis is indeed negligible. An error in the relative semi-major axis, instead, turns into an error in the secular component of the relative motion (a kind of an artificial drift) degrading remarkably the overall accuracy of the model.

Fig. 4 addresses the semi-major axis component only, as being the one responsible for the change in phasing among the chief and the target, showing the evolution of the mean value with respect to the value obtained at the first step $\bar{a}(t_0) = \bar{a}_0$. In the left view all the approaches are depicted, whereas in the right one the focus is on the second order methods. This allows comparing their performances and visualizing the effects introduced by the simplification of terms performed in **E-I**, where the second order $J_2$-solution is not fully consistent as $J_2^2$ terms were neglected everywhere except for in the semi-major axis [22].

## Implemented Algorithm

The implemented algorithm finds its inspiration from the work of Ref. 22, devoted to ground-based LEO orbits monitoring and maintenance. There, the mean OEs are computed through an iterative method cancelling the short-periodic terms due to $J_2$ using Eckstein's theory. And the periodic contributions due to the remaining terms of the geopotential are computed through the Kaula first order method.

In this work the focus is on spaceborne applications, and, in light of the comparison just performed, the second order **A-2nd** method is selected to cancel the effect of the $J_2$, since this provides better accuracy while avoiding a numerical iterative process. In addition, dealing with formation flying, a further refinement is only needed for the semi-major axis component. To this end, the Kaula method is also selected due to the fact that its formulation is very convenient for the recursive implementation of the higher order and degree components. Moreover, given their magnitude, indeed the geopotential terms of order greater than two can be accounted to the first order. The transformations so obtained are labelled **KA-*nxm***, being *n* and *m* respectively order and degree of the geopotential terms accounted in the corrections.

Note that as the algorithm is developed in non-singular elements, there is no need of solving the Kepler's equation in the transformations, which is however needed afterwards to recover

the inertial state from the osculating OE set with mean argument of latitude. Moreover, no problems of singularity arise in the Kaula phase, since this is used only to correct the semi-major axis (e.g., there are no issues due to the $e$ at denominator of the $\Delta e$ part of the eccentricity vector correction, for the cases in which it does not simplify with the $e$ coming from the eccentricity functions). The correction of the semi-major axis requires only the computation of inclination, short-, and long-periodic eccentricity functions but none of their derivatives with respect to their arguments. Finally, being a first order refinement, this is the same in both directions, with the sign related to the direction of transformation.

In the remainder, the algorithm supports the corrections up to order-6 degree-6 (i.e, KA-6x6), with short-periodic eccentricity functions explicitly written up to $e^6$. Dealing with spaceborne implementations one should regard the trade-off between the benefits provided by accounting higher-order terms versus the related computational cost. This topic is further developed in the next section.

**Results**

This section presents the numerical accuracy that can be achieved by adopting the proposed algorithm. To this end, the validation of the propagation of the relative motion is carried out using the guidance set-up of Fig. 1-a) with no additional G&C algorithms (i.e., depicted with white-dashed box). The *reference* states of the deputy and chief satellites $y_{\mathrm{TOD}}$ are obtained expressing in TOD the ones out of the numerical integration in Earth-Mean-Equator (EME) 2000. The modelled state of the deputy $\tilde{y}_{\mathrm{TOD,\,d}}$ is obtained applying the $g\left(f\left(\boldsymbol{x}(t)\right)\right)$ transformation of Eqn 3, where the mean OE set $\boldsymbol{x}(t)$ is computed from the ROEs $\delta\boldsymbol{\alpha}(t)$ as defined in Ref. 2. The relative dynamics at later time is propagated according to:

$$\delta\boldsymbol{\alpha}(t) = \Phi_{\mathrm{M}}(\boldsymbol{x}_0, t_0, \Delta t)\, \delta\boldsymbol{\alpha}_0, \qquad \Delta t = t - t_0 \tag{4}$$

Here $\Phi_{\mathrm{M}}$ is the closed-form State-Transition-Matrix (STM) of the considered model, as follows:

- **M1**: first order expansion of deputy's orbit w.r.t.to the chief, addressing only the secular terms due to $J_2$ to the first order. By exploiting the near-circular orbit assumption, the STM reduces to the one used for the GNC of AVANTI, given in equation (6) of Ref. 5. Note that this corresponds to the STM (A6) in the Appendix of [23], when the terms proportional to $e$ are neglected.
- **M2**: first order expansion of deputy's orbit w.r.t. the chief, addressing the secular terms due to $J_2$, $J_2^2$, $J_4$ and $J_6$. The closed-form STM is given in equation (13) of Ref. 9. It is obtained applying the same state transformation used in [23]; therefore, this STM is valid for whatever eccentricity of the chief's orbit.

The error in relative position and velocity at time $t$ in the TOD frame is given by:

$$\delta\boldsymbol{e}(t) = \tilde{\boldsymbol{y}}_{\mathrm{TOD,\,d}}(t) - \boldsymbol{y}_{\mathrm{TOD,\,d}}(t), \tag{5}$$

since the chief state – assumed to be known with the same accuracy of the reference – cancels out. The symbol $\delta$ is introduced to emphasize that $\boldsymbol{e}$ is a relative quantity. In the following, such error is weighted as:

$$\delta\hat{\boldsymbol{e}} = \mathrm{W}\delta\boldsymbol{e}, \qquad \mathrm{W} = diag(1,1,1,1/n_{c0}, 1/n_{c0}, 1/n_{c0}) \tag{6}$$

using the chief's mean motion $n_{c0}$, to provide an error measured in meters.

In order to assess the accuracy performance of the whole relative motion propagation set-up the index of merit ν over the fixed time duration $\Delta t$ is defined as:

$$\nu_{\Delta t} = \nu(\Delta t) = \max_{t_{0,i}\in[t_0, t_0+\mathrm{T_{ref}}]} \left\| \delta\hat{\boldsymbol{e}}(\Delta t, t_{0,i}) \right\|_2 = \max_i v_i(\Delta t) \tag{7}$$

Accordingly, this index provides the maximum of the norm-2 of the weighted relative error in meters, over the given elapsed time Δt, considering all possible i-th initial times $t_{0,i}$ contained in the reference interval $T_{ref}$ (typically equal to one orbital period). The index of Eqn 7 is inspired from the one defined in equation (8) of Ref. 24 and used to compare the several relative motion models surveyed there. Though, the adopted index extends the one of [24], by considering the effect of the initial conditions, introduced by the osculating/mean elements' conversion errors. This aspect was regarded in the comparative work of Ref. 25, where for each given considered relative orbit, a set of 100 equally spaced initial conditions were propagated. As a result, the metric of Eqn 7 merges two fundamental aspects, namely: the quantitative result of the relative error expressed in meters (beneficial to size GNC hardware and algorithms), and the conservative principle of the worst-case condition (beneficial to provide a realistic assessment of the performance).

The presented analyses are carried out assuming a scenario from the PRISMA (Prototype Research Instruments and Space Mission Technology Advancement) mission [26]. Accordingly, the orbit of the chief is taken as sun-synchronous, dusk-dawn, $e$ = 0.001, and 710 km of height. Moreover, for the inclusion of the effects of the non-conservative perturbations, the deputy and chief satellites are customized on the Tango and Mango spacecraft respectively. The PRISMA scenario has been chosen as representative of LEO orbits with a height where the effect of the differential aerodynamic drag is negligible (see section 7 of Ref. 2). Beyond pure formation flying applications, this orbital area is particularly interesting for future active debris removal activities.

Regarding the relative motion, the two scenarios summarized in Table 1 are considered. There the relative orbits are defined through the relative semi-major axis $\delta a$, relative mean longitude $\delta\lambda$, magnitude of the relative eccentricity vector $\delta\boldsymbol{e}$, and magnitude of the relative inclination vector $\delta\boldsymbol{i}$. An (anti-)parallel relative eccentricity/inclination vector configuration is assumed. The first scenario (i.e., **S1**) presents a bounded trajectory displaced few kilometres away from the chief satellite in along-track direction. Therefore, **S1** corresponds to the N2 case of [24], with relative orbit size of circa 300 m, though displaced in along-track. The second scenario (i.e., **S2**), instead, foresees a drifting relative motion, with larger orbit size, as typically used in the first phases of a far-range rendezvous (though in that case travelled to get closer to the target). **S2** is introduced to investigate the difference between the **M1** and **M2** relative motion models, thought remaining in the domain of validity of the first order OEs expansion approach.

*Table 1: Definition of the relative orbits for each considered scenario.*

| **Scenario** | **\|aδa\| [m]** | **\|aδλ\| [m]** | **\|\|aδe\|\| [m]** | **\|\|aδi\|\| [m]** |
|---|---|---|---|---|
| S1 | 0 | 4500 | 250 | 300 |
| S2 | 200 | 4500 | 1500 | 3000 |

The summary of the performed simulations is provided in Table 2 for the scenario **S1** and Table 3 for the scenario **S2**. For each simulation, the $T_{ref}$ interval is taken as 5940 seconds that corresponds to circa the unperturbed orbital period of the chief satellite. By considering a time granularity of 1 minute for the initial times $t_{0,i}$, a population of 99 different initial conditions is employed for each run. The value of the index ν is provided for two simulation legs, corresponding to 1-day (i.e., 14.5 $T_{ref}$) and 2-day long (i.e., 29 $T_{ref}$) time durations.

In the cases of Table 2 the propagation of the relative motion adopts the STM of the model **M1** for all the simulations. The osculating/mean OEs conversions, instead, make use of the different approaches listed in the first column (i.e., Transf.). The *reference* orbits are generated for three different orbital dynamics. In the first two cases the non-homogenous

Earth mass distribution is the solely perturbation accounted, respectively geopotential of order-6 degree-6 and order-30 and degree-30. In the last case, in addition to the 30 by 30 geopotential all other orbital perturbations are included (e.g., aerodynamic drag, solar radiation pressure, third-body due to Moon and Sun, tidal and relativity effects). In all these three cases the *reference* orbits of the chief and deputy satellites are obtained with numerical integration in the EME2000 reference system. Finally, for each performed simulation the reference to the related plot is recalled (i.e., see the columns Ref. in Tables 2 and 3).

*Table 2: Summary of performed simulations for the Scenario 1.*
*Index scores are given for the model M1.*

| Transf. | Geopot. 6x6 | | | Geopot. 30x30 | | | Geopot. 30x30 & Others | | |
|---|---|---|---|---|---|---|---|---|---|
| | Ref. | $\nu_{1day}$ [m] | $\nu_{2day}$ [m] | Ref. | $\nu_{1day}$ [m] | $\nu_{2day}$ [m] | Ref. | $\nu_{1day}$ [m] | $\nu_{2day}$ [m] |
| M-1st | Fig. 5.a | 46.50 | 61.51 | - | - | - | - | - | - |
| A-2nd | Fig. 5.b | 20.69 | 41.29 | - | - | - | - | - | - |
| KA-4x4 | Fig. 6.a | 16.19 | 31.12 | Fig. 7.a | 20.82 | 41.64 | Fig. 8.a | 36.05 | 106.76 |
| KA-6x6 | Fig. 6.b | 1.08 | 1.70 | Fig. 7.b | 14.25 | 28.14 | Fig. 8.b | 31.57 | 99.30 |

The results of the comparison of different transformation methods in the osculating/mean conversions when dealing with the orbital dynamics perturbed by a degree-6 order-6 gravity field are presented in Fig. 5 and Fig. 6. The 99 cases are highlighted through different colours, and the y-axis shows the trend over time of each corresponding $v_i(\Delta t)$ as defined in Eqn 7. A remarkable improvement is already achievable by including $J_2$ to the second order, as shown in the two views of Fig. 5. Then, a further improvement can be achieved with the full proposed algorithm, reaching the best possible performance in the case where the transformations account for the same geopotential terms of the environment (i.e., 6 by 6). In such limit case, the fully analytical propagation of the relative motion would remain accurate at meter level even after 2 days.

Once verified the effectiveness of the proposed approach, the remaining simulations address the trade-off between transformation complexity (i.e., KA-4x4 or KA-6x6) and achievable accuracy performance when the dynamics resembles a more realistic environment.

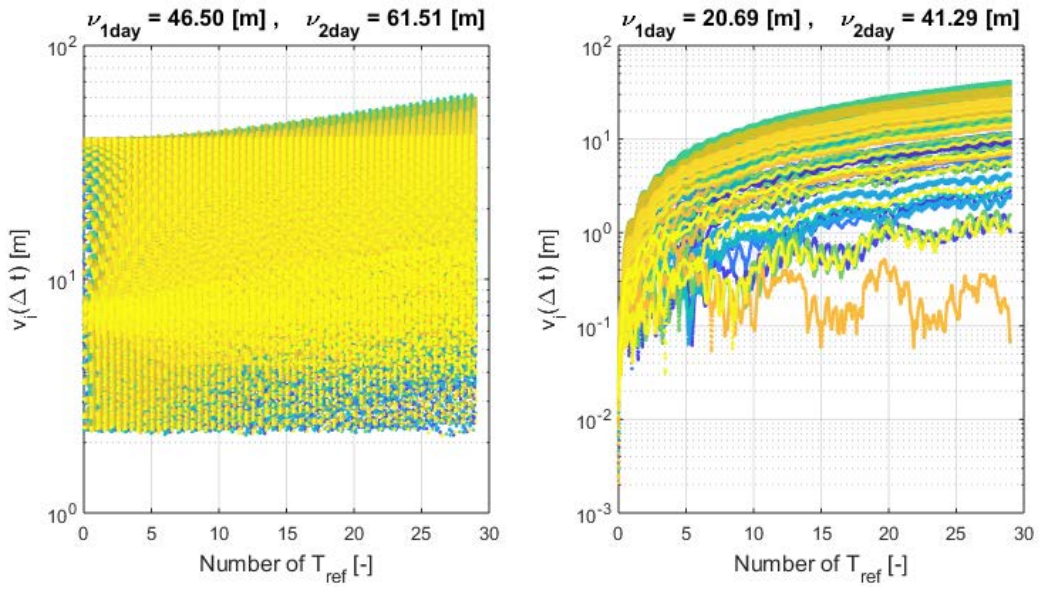


a) M-1st b) A-2nd

*Fig. 5: Reference orbits from numerical propagation in 6x6 gravity field.*

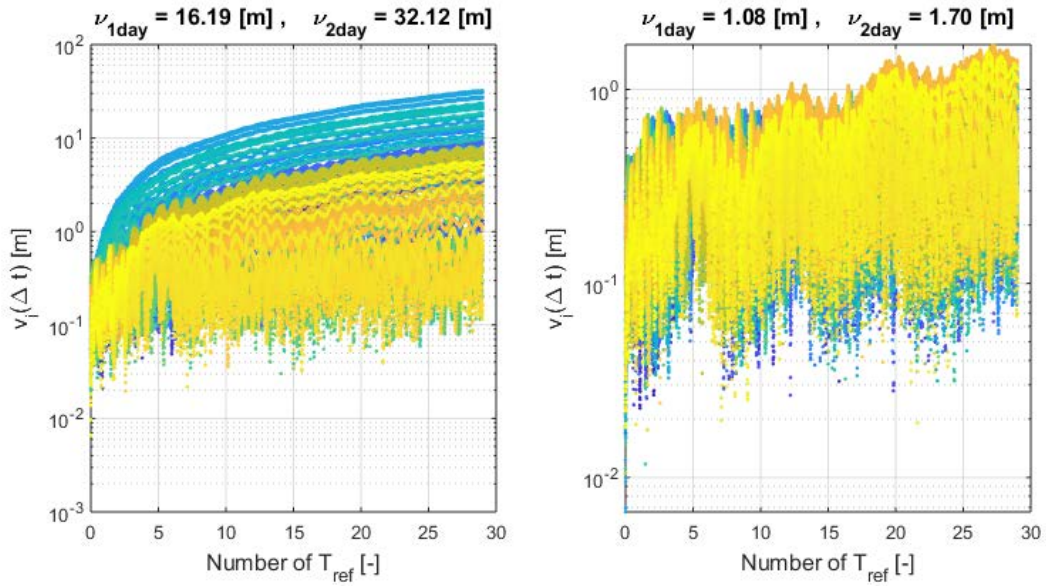


a) KA-4x4 b) KA-6x6

*Fig. 6: Reference orbits from numerical propagation in 6x6 gravity field.*

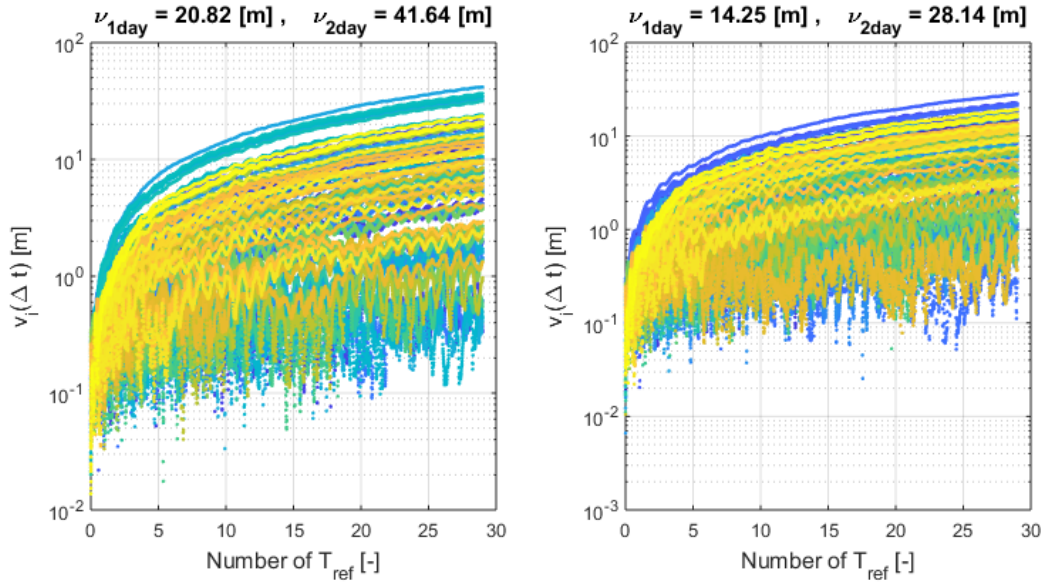


a) KA-4x4 b) KA-6x6

*Fig. 7: Reference orbits from numerical propagation in 30x30 gravity field.*

By reading the results for each line of Table 2, it is possible to measure the degradation effect brought by higher terms of the potential and remaining orbital perturbations. For the latter contribution, the modelling error is also due to the lack of inclusion of the perturbations in the relative motion model. The related plots for the dynamics simply perturbed by a degree-30 order-30 gravity field and by the general perturbed case are respectively shown in Fig. 7 and Fig. 8.

The simulation results collected in Table 3 concern the relative orbit of scenario **S2**. In all these cases, the adopted osculating/mean OE conversion method is the **KA-6x6**. The first row presents the results obtained by modelling the relative motion with the **M1** STM. By looking at the values obtained in the 6 by 6 gravity field, the marginal improvement achieved by **M2** can be appreciated. In this situation, in fact, since the transformations account for all the geopotential terms of the environment, it is possible to isolate the tiny relative effect of the higher zonal terms, for this size of relative motion.

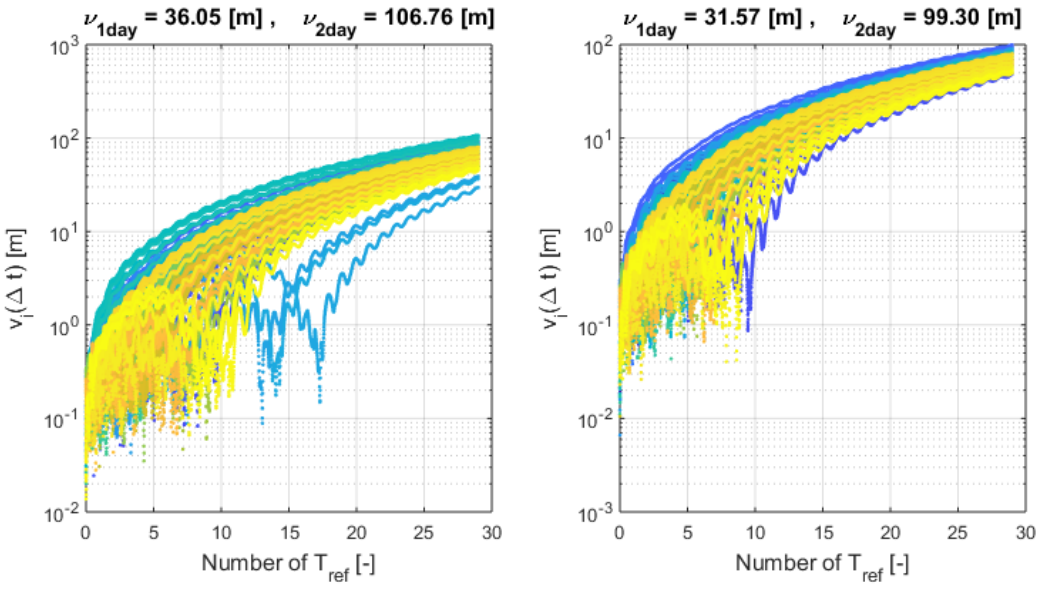


a) KA-4x4 b) KA-6x6

*Fig. 8: Reference orbits from numerical propagation in 30x30 gravity field and remaining orbital perturbations.*

*Table 3: Summary of performed simulations for the Scenario 2. Osculating/mean transformations with KA-6x6 only.*

| Model | Geopot. 6x6 | | | Geopot. 30x30 | | | Geopot. 30x30 & Others | | |
|---|---|---|---|---|---|---|---|---|---|
| | Ref. | $\nu_{1day}$ [m] | $\nu_{2day}$ [m] | Ref. | $\nu_{1day}$ [m] | $\nu_{2day}$ [m] | Ref. | $\nu_{1day}$ [m] | $\nu_{2day}$ [m] |
| M1 | Fig. 9.a | 7.45 | 13.69 | - | 16.57 | 33.65 | Fig. 10.a | 33.96 | 102.11 |
| M2 | Fig. 9.b | 6.88 | 12.43 | - | 17.38 | 34.04 | Fig. 10.b | 34.77 | 104.44 |

Indeed the **M2** model provides an elegant and compact formulation to account for the general geopotential field. Nevertheless, in the generally perturbed case and in the considered relative motion domain (limited in size to use a model based on first order expansion w.r.t. the chief orbit) its improvement in accuracy is nullified by the error introduced by the remaining neglected perturbations. The plots related to these results are Fig. 9 and Fig. 10. Depending on the required accuracy, one should consider either to improve the model of the relative dynamics (e.g., also accounting for the perturbations currently not considered) or, at engineering level, it would not be justified the increase of complexity of the code of **M2** compared to **M1**.

## Conclusion

This paper presented an algorithm to perform the two-may mean/osculating orbital elements' transformations as required to support a relative orbital elements-based relative GNC system when the orbit of the chief satellite is known in an inertial frame. The treatment is confined into the low Earth orbit region with focus on the orbital perturbation due to the non-homogenous terrestrial mass distribution.

The proposed approach combines a Hamiltonian technique applied to the $J_2$ problem with Kaula's linear perturbation method for the remaining terms of the geopotential. The resulting algorithm is compact, fully analytical in both transformation directions, and free from singularities (but not applicable in the vicinity of the critical inclination). Thus it can serve a wide range of formation flying and active debris removal applications.

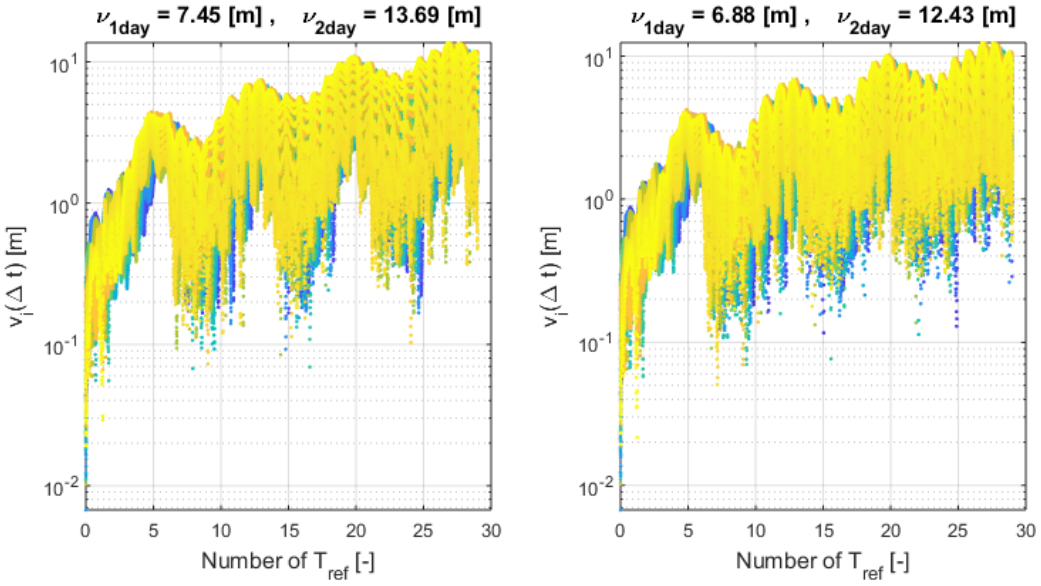


a) Model M1 b) Model M2

*Fig. 9: Reference orbits from numerical propagation in 6x6 gravity field.*

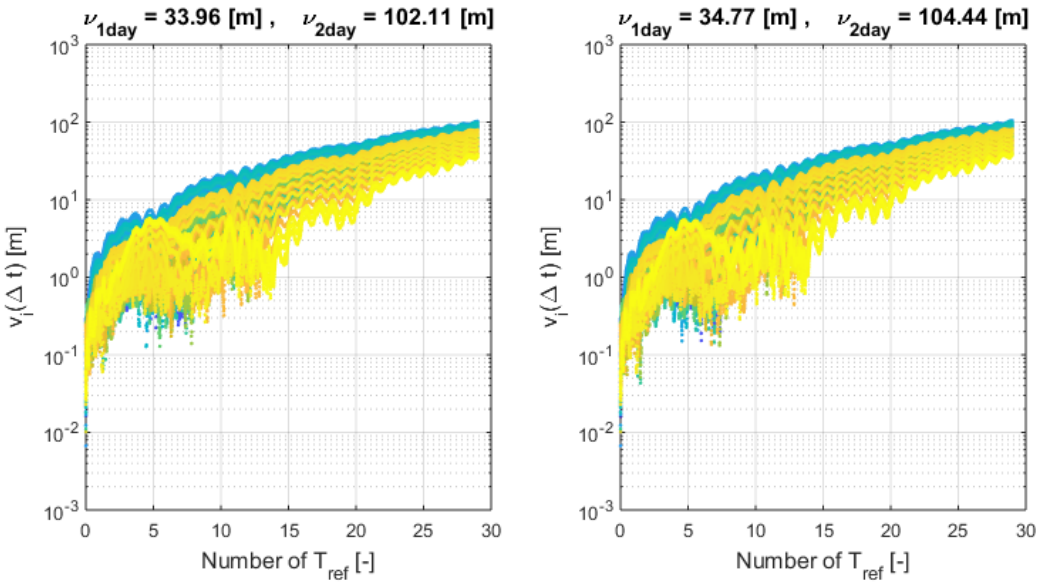


a) Model M1 b) Model M2

*Fig. 10: Reference orbits from numerical propagation in 30x30 gravity field and remaining orbital perturbations.*

The exploitation of the proposed algorithm improves the accuracy performances of analytical orbital elements-based relative motion models. To prove this, the paper presented the achievable relative position error results, depending on the geopotential terms accounted in the transformations, for 1-day and 2-day long propagation legs, into a high fidelity simulation environment. Accordingly, this analysis provides a realistic assessment of the achievable propagation performance, regardless the initialisation conditions. Moreover, with concern to spaceborne implementations, this analysis allows understanding what level of complexity is required to be included in the code, depending on the actual accuracy that is required by the mission task (e.g., GNC algorithm, sensors a/o actuator capabilities).

**Acknowledgments**

This project has received funding from the European Research Council (ERC) under the European Union's Horizon 2020 research and innovation programme (grant agreement No 679086-COMPASS).

**References**

1. Gim, D.-W. and Alfriend, K.T., "State Transition Matrix of Relative Motion for the Perturbed Noncircular Reference Orbit", *Journal of Guidance, Control, and Dynamics*, Vol. 26, No. 6, 2003, pp. 956–971.

2. Gaias, G., Ardaens, J.-S., and Montenbruck, O., "Model of J2 Perturbed Satellite Relative Motion with Time-Varying Differential Drag", *Celestial Mechanics and Dynamical Astronomy*, Vol. 123, No. 4, 2015, pp. 411–433.

3. Schaub, H. and Junkins, J.L., *Analytical Mechanics of Space Systems*, AIAA, Reston, Virginia (USA), 2014, Chap. 14.

4. Gim, D.-W., and Alfriend, K.T., "Criteria for Best Configuration and Sub-Optimal Reconfiguration for MMS Mission", *Proceedings of the AAS Spaceflight Mechanics Meeting*, AAS Paper 04-152, Maui, HI, 2004.

5. Gaias, G. and Ardaens, J.-S., "Flight Demonstration of Autonomous Noncooperative Rendezvous in Low Earth Orbit", *Journal of Guidance, Control, and Dynamics*, Vol. 41, No. 6, 2018, pp. 1337–1354.

6. Gill, E., and Montenbruck, O., "Comparison of GPS-based Orbit Determination Strategies", *Proceedings of the 18th International Symposium on Space Flight Dynamics*, SP-548, ESA, Noordwijk, The Netherlands, 2004, pp. 169–174.

7. Zhong, W. and Gurfil, P., "Mean Orbital Elements Estimation for Autonomous Satellite Guidance and Orbit Control", *Journal of Guidance, Control, and Dynamics*, Vol. 36, No. 6, 2013, pp. 1624–1641.

8. Wnuk, E., "Recent Progress in Analytical Orbit Theories", *Advances in Space Research*, Vol. 23, No. 4, 1999, pp. 677–687.

9. Gaias, G. and Colombo C., "Semi-Analytical Framework for Precise Relative Motion in Low Earth Orbits", *7th International Conference on Astrodynamics Tools and Techniques* (ICATT), DLR Oberpfaffenhofen, Germany, 2018.

10. Kaula, W.M., *Theory of Satellite Geodesy*, Blaisdell publ. Co., Wahhman, Mass. (1966).

11. Brouwer, D., ''Solution of the Problem of Artificial Satellite Theory Without Drag'', *Astronautical Journal*, Vol. 64, No. 1274, 1959, pp. 378 397.

12. Lyddane, R.H., "Small Eccentricities or Inclination in the Brouwer Theory of the Artificial Satellite", *Astronautical Journal*, Vol. 68, No. 8, 1963, pp. 555-558.

13. Cain, B.J., "Determination of Mean Elements for Brouwer's Satellite Theory", *Astronomical Journal*, Vol. 67, No.6, 1962, pp. 391-392.

14. Walter, H.G., “Conversion of Osculating Orbital Elements into Mean Orbital Elements”, Astronomical Journal, Vol. 72, No. 8, 1967, pp. 994-997.

15. Eckstein, M.C. and Hechler, H., “A reliable derivation of the perturbations due to any zonal and tesseral harmonics of the geopotential for nearly-circular satellite orbits”, *ESOC Technical Note*, ESRO SR-13, 1970.

16. Ustinov, B.A., “Motion of Satellites along low-eccentricity Orbits in a noncentral terrestrial gravitational Field”, *Cosmic Research*, Vol. 2, 1967, pp.184-193 (in Russian).

17. Deprit, A., “Canonical transformations depending on a small parameter”, *Celestial Mechanics*, Vol. 1, No. 1, 1969, pp. 12-30.

18. Deprit, A., “The elimination of the parallax in satellite theory”, Celestial Mechanics, Vol. 24, No. 2, 1981, pp. 111-153.

19. Lara, M., San-Juan, J.F., and López-Ochoa, L.M., “Proper Averaging Via Parallax Elimination”, paper (AAS 13-722) *Advances in the Astronautical Sciences*, Vol. 150, 2014, pp. 315-331.

20. Lara, M., San-Juan, J.F., and López-Ochoa, L.M., “Delaunay variables approach to the elimination of the perigee in Artificial Satellite Theory”, Celestial Mechanics and Dynamical Astronomy, Vol. 120, No. 1, 2014, pp. 39-56.

21. Deprit, A., “Delaunay normalisations”, Celestial Mechanics, Vol. 26, 1982, pp. 9-21.

22. Spiridonova, S., Kirschner, M., and Hugentobler, U., “Precise Mean Orbital Elements Determination for LEO Monitoring and Maintenance”, *24th International Symposium on Space Flight Dynamics ISSFD*, Laurel, Maryland, USA, 2014.

23. Koenig, A.W., Guffanti, T., and D’Amico, S., “New State Transition Matrices for Spacecraft Relative Motion in Perturbed Orbits”, *Journal of Guidance, Control, and Dynamics*, Vol. 40, No. 7, pp. 1749-1768, 2017.

24. Sullivan, J., Grimberg, S., and D’Amico, S., “Comprehensive Survey and Assessment of Spacecraft Relative Motion Dynamics Models”, *Journal of Guidance, Control, and Dynamics*, Vol. 40, No. 8, pp. 1837-1859, 2017.

25. Alfriend, K. T., and Yan, H., “Evaluation and Comparison of Relative Motion Theories”, *Journal of Guidance, Control, and Dynamics*, Vol. 28, No. 2, pp. 254-261, 2005.

26. Persson, S., Jakobsson, B., Gill, E., “PRISMA – Demonstration Mission for Advanced Rendezvous and Formation Flying Technologies and Sensors”, No. 05-B56B07, *56th International Astronautical Congress IAC*, Fukuoka, Japan, 2005.